https://doi.org/10.5194/egusphere-2026-3518
Preprint. Discussion started: 3 July 2026

Mixing states and composition of fine aerosol particles in the 2023 Canadian wildfire plumes detected in southern Greenland

Kouji Adachi[1*], Nora Bergner[2], Joanna Alden[2, a], Julia Schmale[2], Sho Ohata[3], Yutaka Tobo[4,5]

[1] Department of Atmosphere, Ocean, and Earth System Modeling Research, Meteorological Research Institute, Tsukuba, Japan
[2] Extreme Environments Research Laboratory, Ecole Polytechnique Fédérale de Lausanne, Sion, Switzerland
[3] Institute for Space–Earth Environmental Research, Nagoya University, Nagoya, Japan
[4] National Institute of Polar Research, Tachikawa, Japan
[5] Graduate Institute for Advances Studies, SOKENDAI, Tachikawa, Japan
[a] now at: Université Savoie Mont Blanc, INRAE, CAARTEL, Thonons-Les-Bains, 74200, France

Correspondence to: Kouji Adachi (adachik@mri-jma.go.jp)

Abstract. Rapid climate change has driven an increase in extreme wildfire activity. In 2023, huge wildfires occurred in Canada. Smoke generated by the wildfires was exceptionally severe and was transported to Europe and Eurasia across Greenland. Despite their importance for understanding the global climate, studies investigating aerosols, particularly their mixing states and composition, within the wildfire plumes remain limited. Greenland is an ideal location for studying long-range transport of the Canadian wildfire smoke because of the minimal influence of local wildfire and anthropogenic emissions. In this study, atmospheric observations were conducted in southern Greenland during the summer of 2023. Fine-mode aerosol particles were analyzed using transmission electron microscopy to characterize their mixing states and composition at the individual particle level. The influence from the Canadian wildfire smoke, characterized by an increased abundance of carbonaceous and potassium sulfate particles, was observed when the sampled air mass originated from an area affected by wildfires, contrasting from samples from the background period, which was characterized by sea salt and sulfate. In contrast to the observations from fresh wildfires in previous campaigns that detected many spherical organic particles (tarballs), the carbonaceous particles from the Canadian wildfire were predominantly composed of organic materials embedding numerous small soot particles and potassium sulfate. These samples demonstrate mixing states and individual particle composition of aged aerosol particles from large wildfire plumes that had travelled long distance. This information has implications for interpreting their optical properties and aging processes during long-range transport in the Arctic.

https://doi.org/10.5194/egusphere-2026-3518
Preprint. Discussion started: 3 July 2026

1. Introduction

The Arctic climate is rapidly changing, warming nearly four times faster than the global average (Rantanen et al., 2022). In recent years, sea ice coverage, glaciers, and ice sheets in the Arctic have been shrinking (Meier & Stroeve, 2022; Mouginot et al., 2019). Changes in the cryosphere have resulted in an expansion of vegetation and snow- and ice-free land along the Arctic coast, leading to an increase in natural aerosol emissions (Schmale et al., 2024). Conversely, long-range transported anthropogenic aerosol particles are projected to decline due to regulations on aerosol emissions from human activities in mid-latitudes (Schmale et al., 2022; Sharma et al., 2019). Consequently, the relative contributions of aerosol particles emitted from natural sources, such as sea spray aerosols from the ocean, mineral dust aerosols from glacial washout plains, and bioaerosols from vegetated tundra are expected to increase in the Arctic Atmosphere (Tobo et al., 2019, 2024; Schmale et al., 2021; Freitas et al., 2023, 2024). In addition, as the climate warms, the size, frequency, and intensity of wildfires in high-latitude regions are expected to increase (Descals et al., 2022; McCarty et al., 2021), thereby enhancing the importance of wildfire-derived aerosols in the Arctic atmosphere.

Wildfire emissions have a substantial impact on both the climate system (Keywood et al., 2013) and human health (Matz et al., 2020). Wildfires emit large amounts of CO_2, soot (or black carbon), ash, brown carbon, including tarballs, and other gases and aerosols (Andreas, 2019; Adachi et al., 2022; Yokelson et al., 2009). Tarballs, for example, are a type of brown carbon aerosols that absorb light and are predominantly emitted from wildfires (Chakrabarty et al., 2023; Sedlacek et al., 2018; Adachi et al., 2024). Soot particles are also significantly emitted during wildfires and contribute to aerosol light absorption, as well as to the lofting wildfire smoke into the stratosphere through plume heating (Yu et al., 2019). The extent of light absorption by soot particles depends on their atmospheric abundance, particle size and composition, and how different components are internally mixed within individual particles (i.e., mixing states) (Chen et al., 2025; Adachi et al., 2010). Additionally, soot particles deposited on the Greenland ice sheet contribute to the melting of the Greenland ice sheet by altering the ice albedo (Thomas et al., 2017; Skiles et al., 2018). A study of ice core measurements showed that historical widespread melt events of the Greenland ice sheet were caused not only by increasing temperature but also by soot deposition from forest fires (Keegan et al., 2014). Moreover, recent ship-based measurements have indicated that aerosols from wildfires can serve as efficient ice-nucleating particles over the Arctic Ocean, potentially influencing glaciation of Arctic mixed-phase clouds (Sato et al., 2025; Taketani et al., 2025).

Canada experienced an unprecedented wildfire season in the summer of 2023. The wildfires burned intensely across multiple regions from late April to October due to the hottest and driest conditions in northwestern Canada for 40 years (Wu et al., 2025; Luo et al., 2025). The total area affected by the fires is estimated to be approximately 15 million hectares (Jain et al., 2024). The wildfire emitted vast amounts of gases and aerosols into the atmosphere, causing adverse health effects and decreases in surface air temperature (Roșu et al., 2025; Zhang et al., 2025; Flood et al., 2025; Byrne et al., 2024; Wang et al., 2024). It is estimated that the total carbon emissions from the 2023 Canadian wildfires were 647 TgC (Byrne et al., 2024). Pollution plumes travelled over the Northern Hemisphere, reaching Europe and Eurasia across Greenland (Hu et al., 2025; Masoom et al., 2025; Zhang et al., 2025). These plumes were observed at altitudes greater than 4,000 m, peaking at over 10,000 m above Europe (Hu et al., 2025). A small fraction of the plume was also injected into the lower stratosphere (Khaykin et al., 2025; Zhang et al., 2024).

The current study investigated individual aerosol particles collected in southern Greenland during the summer of 2023 as part of the multidisciplinary campaign, *Greenlandic Fjord ecosystems in a changing climate: Socio-cultural and environmental interactions* (*GreenFjord*). Measurements of individual aerosol particles focusing on mixing states and composition are limited in southern Greenland (Adachi et al., 2021, 2023; Kikuchi et al., 1996). Aerosol particles smaller than 700 nm in aerodynamic diameter were analyzed using transmission electron microscopy (TEM), enabling particle-resolved characterization of their shapes and constituents. During the campaign, southern Greenland experienced significant influence from long-range transported smoke originating from the record-breaking Canadian wildfires, providing a unique opportunity

https://doi.org/10.5194/egusphere-2026-3518
Preprint. Discussion started: 3 July 2026

to examine aged aerosols from wildfire plumes that had undergone atmospheric processing during transport to the Arctic. This study focuses on contrasting fine-mode aerosol populations observed during background conditions and wildfire plume periods. This study aims to improve understanding of aerosol aging processes, optical properties, and potential climate impacts associated with long-range transported wildfire emissions, as well as background Arctic conditions, from an individual particle perspective.

2. Materials and methods

2.1 Sampling

The GreenFjord campaign aimed to understand the Greenlandic fjord environment, including the cryosphere, ocean, biodiversity, land, and atmosphere, as well as the people living in the fjords. The atmosphere cluster in the GreenFjord campaign focused on measuring the dominant sources of aerosols in southern Greenland, a region characterized by terrestrial vegetation in summer and a unique, highly productive fjord ecosystem. Alden et al. (2026) reported an overview of ground-based and balloon-borne measurements of aerosol number concentrations, size distributions, and aerosol climate-relevant properties (cloud condensation nuclei number concentrations, absorption and scattering coefficients) as well as meteorological conditions during the campaign. Bergner et al. (2026) also reported on ice-nucleating particles in the region during the campaign. Atmospheric measurements including aerosol sampling were conducted from June 16 to August 5, 2023 at the Narsaq International Research Station (NIRS; 60.92° N, 46.05° W, 17 m a.s.l.), located in the subarctic coastal fjord town of Narsaq with a population of ~1,300. During the sampling period, the average surface air temperature was 10.4°C, which was higher than usual (6.2°C–9.9°C during the summers of 2013–2023), and the average relative humidity was 84 %, ranging from 40 % to 100 % (Alden et al., 2026).

From July 4 to August 4, we collected 155 aerosol samples for TEM analysis with a two-hour sampling time for every four hours. Ambient air was introduced to a two-stage impactor sampler (AW-24, Arios) via an electrically conductive tube (~1 m) without a dryer. The sampler had two disks for fine- and coarse-mode sampling, and each held 24 TEM grids (Formvar 200 mesh Cu grids, EM-Japan). The disks rotated on a preset timer and were manually changed every four days. The sampler had a flow rate of 1 L min^{-1}, resulting in aerosol sampling on the fine-mode stage with aerodynamic diameters between 300 and 700 nm (the lower and upper 50 % cutoff sizes, respectively). Particles larger than 700 nm in aerodynamic diameter were also collected on the coarse-mode stage of the same impactor sampler, which we did not use in this study. Samples from July 8, 02:00 to July 11, 14:00 and from July 21, 10:00 to July 23, 14:00 (UTC) were unavailable due to a technical issue. Similar sampling system has been used in our previous studies (e.g., Adachi et al., 2025a).

2.2 Transmission electron microscopy analysis

The shape, size, and composition of individual aerosol particles were analyzed using a transmission electron microscope (JEM-1400, JEOL) equipped with an energy-dispersive X-ray spectrometer (EDS; X-MAX 80, Oxford Instruments). For each grid, particles within a representative area of approximately 670 μm² were analyzed using scanning transmission electron microscopy (STEM) mode with EDS. This area was selected based on TEM images that covered nearly all particles collected on the grid. Particles with an area-equivalent diameter greater than 0.19 μm (corresponding to more than 100 pixels in a STEM image) were identified in STEM dark-field images by applying contrast thresholds between particles and the substrate (Adachi et al., 2019). In total, 16,917 particles from 155 TEM grids were analyzed. Using an acceleration voltage of 120 kV and an acquisition time of 20 seconds, the relative weight percentages of 21 selected elements (C, N, O, Na, Mg, Al, Si, P, S, Cl, K, Ca, Ti, V, Cr, Mn, Fe, Ni, Zn, Sr, and Ba) and the area-equivalent diameters were measured. The detection limit was approximately 0.02 weight percent, based on one standard deviation of the measured intensity.

https://doi.org/10.5194/egusphere-2026-3518
Preprint. Discussion started: 3 July 2026

The measured particles were classified into six categories based on their composition using the classification flowchart in Fig. 1: 1) Mineral dust particles, 2) Sea salt particles, 3) Potassium (K)-bearing particles, 4) Sulfate particles, 5) Carbonaceous particles, and 6) Others. Their predominant chemical forms are 1) aluminosilicate, 2) sodium chloride/sulfate, 3) potassium sulfate, 4) ammonium sulfate, and 5) organic material. Note that the measured particles are mostly internally mixed with several components, and this classification prioritizes primary particles over secondary particles. Therefore, this method could underestimate the mass of secondary aerosol species (e.g., sulfate and organic aerosols), when they are present on the surfaces of mineral dust or sea salt.

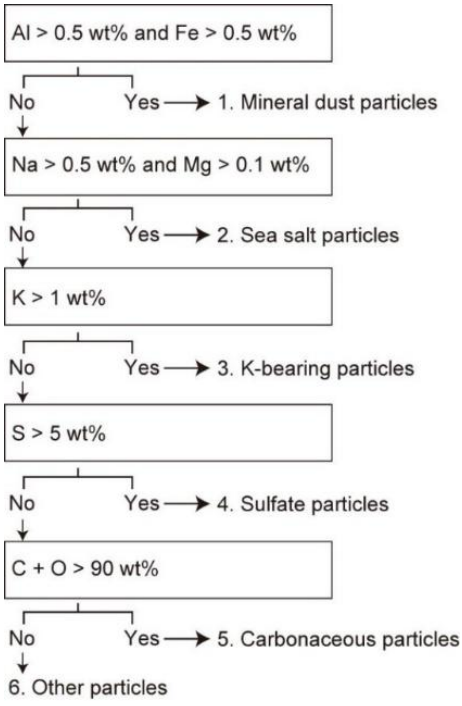

Figure 1. Flow chart for classifying measured particles. Weight percentage values were obtained using scanning transmission electron microscopy with an energy dispersive X-ray spectrometer (STEM-EDS).

2.3 Aerosol mass concentration estimate and carbon monoxide measurement

We obtained atmospheric particle number concentrations and size distributions between 0.19 µm and 93 µm using an optical particle counter (fine dust measuring device; FIDAS, Palas) (Bächler et al., 2021; Fang et al., 2023). To estimate the mass concentration of particulate matter less than 1.0 µm ($PM_{1.0}$) for each four-hour TEM sampling period, we first calculated the total volume of particles with diameters between 0.191 and 1.0 µm measured by FIDAS. Then, we estimated the average particle density using the TEM composition analysis and the resulting number fractions, along with the approximate densities from Adachi et al. (2024): 1) mineral dust (2.7 g cm^{-3}), 2) sea salt (NaCl, 2.16 g cm^{-3}), 3) K-bearing salt (K_2SO_4, 2.66 g cm^{-3}), 4) sulfate ($(NH_4)_2SO_4$, 1.7 g cm^{-3}), 5) carbonaceous particles (1.4 g cm^{-3}), and 6) other particles (2.0 g cm^{-3}). This estimation assumes that the aerosol number fractions measured by STEM-EDS represent the mass fractions of the $PM_{1.0}$ measured at the same time. We applied the average density to the particle volumes to calculate the $PM_{1.0}$ mass concentration (µg m^{-3}) during the sampling period.

The dry carbon monoxide (CO) mixing ratio was measured using a portable, medium-range, infrared laser-based gas analyzer (Pico Series, Aeris Technologies, Inc.).

https://doi.org/10.5194/egusphere-2026-3518
Preprint. Discussion started: 3 July 2026

2.4 Backward trajectory analysis

The hybrid single-particle Lagrangian integrated trajectory (HYSPLIT) transport and dispersion model and the READY website provided by the NOAA Air Resources Laboratory (ARL) were used to estimate the origin of the sampled air masses. The model used a seven-day duration and a quarter-degree Global Forecast System (GFS) archive. The ensemble of backward trajectories with 27 members starting from the NIRS at an altitude of 500 m was calculated. Relatively strong active fires with a fire radiative power (FRP) greater than 100 in MODIS/Aqua occurring within ten days prior to the start of the trajectories were obtained from NASA's Fire Information for Resource Management System to estimate the major burning areas (NASA FIRMS, 2025).

3. Results and discussion

3.1 Influences of Canadian wildfire plumes during the sampling period

In the current study, we divided the sampling period into background air and wildfire plume periods. Alden et al. (2026) classified the campaign period into four categories: (1) background, (2) wildfire plume events, (3) new particle growth events, and (4) fresh pollution. In this study, we do not consider categories (3) and (4) because new particle growth events are typically related to particles smaller than 100 nm, which are smaller than the particles we targeted in our TEM aerosol sampling. Fresh pollution occurred as short-lived spikes from local pollution events lasting less than one hour, which is shorter than our TEM sampling time. Nevertheless, we sometimes observed that large soot particles, which possibly originated from local sources, such as traffic and domestic activities, were externally mixed with sea salt and sulfate-dominated samples.

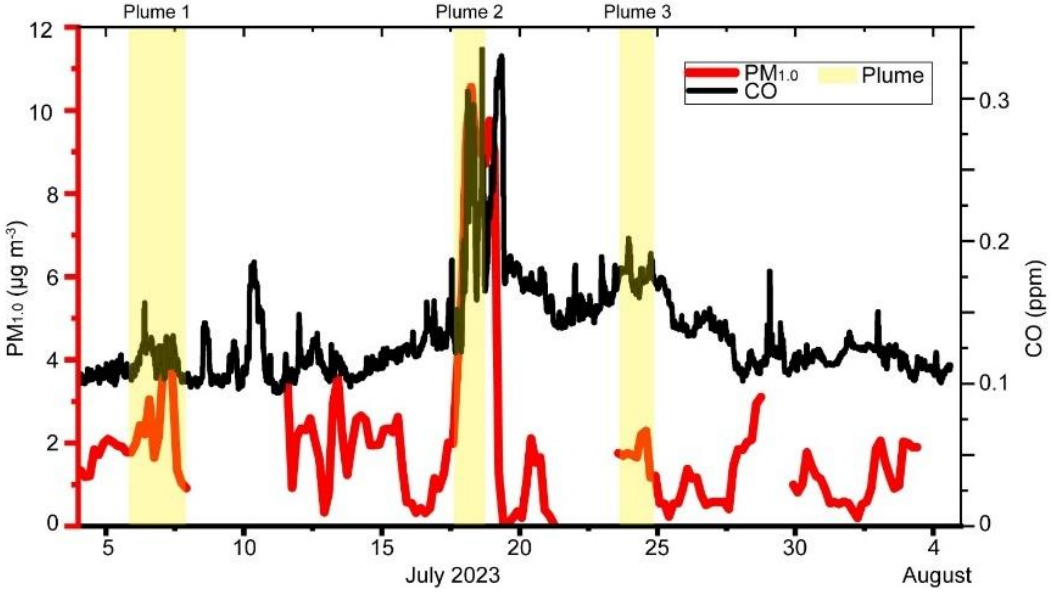

Figure 2. Concentrations of $PM_{1.0}$ (red) and CO (black) during the TEM sampling period. Estimated wildfire plume periods are highlighted. $PM_{1.0}$ data are missing for the following periods due to a lack of TEM results or FIDAS data: from July 8 2:00 to July 11 10:00; from July 21 10:00 to July 23 10:00; and from July 29 2:00 to July 29 18:00 (UTC).

CO and $PM_{1.0}$ concentrations were relatively low during the background periods and increased occasionally during wildfire plume events (Fig. 2). The influence from Canadian wildfire plumes was observed from July 5, 22:13 to July 8, 03:42 (Plume 1) and from July 17, 13:47 to July 18, 20:17 (Plume 2) (UTC) at NIRS during our sampling period (Alden et al., 2026).

https://doi.org/10.5194/egusphere-2026-3518
Preprint. Discussion started: 3 July 2026

A large wildfire plume also arrived at the site between June 27 and 29; however we were unable to collect samples from this plume because it arrived before we started sampling. During these two wildfire plume periods, the concentrations of $PM_{1.0}$ and CO increased to >3 μg m^{-3} and >0.15 ppm, respectively. Additionally, the period from July 23 to 25 showed an increase in CO concentrations (>0.15 ppm) with a modest enhancement in $PM_{1.0}$ concentration (~2 μg m^{-3}). Based on the elevated CO concentrations, aerosol composition, and model results, which will be discussed later, we also considered this period to be a wildfire plume that we focus on in this study (Plume 3; from July 23, 14:00 to July 25, 02:00 in UTC). A peak in CO concentration (~0.18 ppm) was observed on 10 July; however, this period was excluded from the analysis due to the lack of TEM samples.

To verify the influence of the wildfire plumes during these periods, we simulated seven-day backward trajectories (Fig. 3). The results showed that representative air parcels travelled over large wildfires in Quebec for all three plumes. In addition, some trajectories in Plume 1 travelled over wildfires in Saskatchewan. There was continuous wildfire activity in these regions during the summer (Jian et al., 2024). Thus, we conclude that these three periods were affected by plumes from the Canadian wildfires. Outside of these periods, the air at the sampling point was considered background air, although it is probable that a stagnant, persistent, diluted wildfire plume could have influenced the background air.

In addition to the backward-trajectory analysis, we evaluated the aerosol distributions using a global aerosol emission and distribution model (Model of Aerosol Species in the Global Atmosphere; MASINGAR) provided by the Meteorological Research Institute and the Japan Meteorological Agency (MRI/JMA) (Yumimoto et al., 2017) (Fig. S1). The model showed substantial transport of organic and black carbon from the Canadian wildfires on July 7, 8, 17, and 18, which is consistent with the backward-trajectory model and the CO and $PM_{1.0}$ observations from Plumes 1 and 2. On July 24 (Plume 3), a diluted plume from the Canadian wildfires was transported to the sampling site, although it was less clear than in Plumes 1 and 2. Overall, the trajectories and model results, as well as the CO and $PM_{1.0}$ observations, support the hypothesis that the sampling site was considerably influenced by the Canadian wildfires.

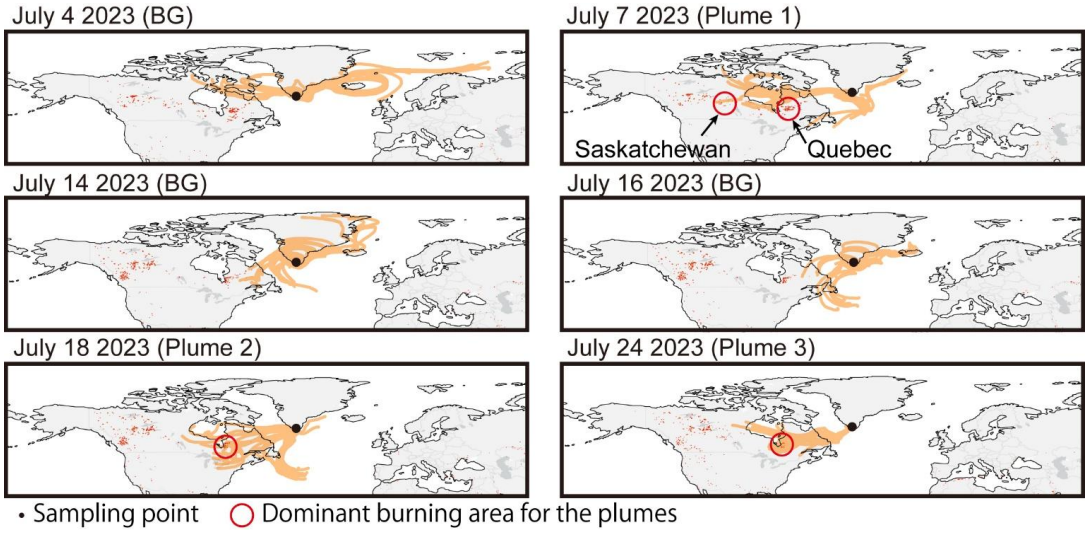

Figure 3. Possible influences of Canadian wildfires on the sampling area during representative sampling periods. Ensemble seven-day backward trajectories starting from the Narsaq International Research Station (solid black dot) at an altitude of 500 m are shown as orange lines. Red dots indicate active fires. The dominant burning areas that possibly influenced the sampling area are shown in red circles. A light gray canvas (WGS84) web map from NASA FIRMS was used (https://firms.modaps.eosdis.nasa.gov/). The backward trajectory start times are at 00:00 (UTC). The periods of July 7, 18, and 24 cover the wildfire plume periods. BG: background period.

https://doi.org/10.5194/egusphere-2026-3518
Preprint. Discussion started: 3 July 2026

3.2 Number fraction and size dependence of aerosol types

The composition of individual particles was measured using a STEM-EDS system and classified based on their characteristic elements (Fig. 1). The average number fractions of all samples for mineral dust, sea salt, K-bearing particles, sulfate particles, carbonaceous particles, and other particles were 1 %, 29 %, 10 %, 16 %, 41 %, and 3 %, respectively. Samples from the wildfire plumes had higher fractions of carbonaceous (57 %) and K-bearing (15 %) particles than samples from the background period (37 % and 9 %, respectively) (Fig. 4). Conversely, samples from the background period contained higher fractions of sea salt (33 %) and sulfate (16 %) particles than samples from the wildfire plume period (13 % and 12 %, respectively). The fractions of mineral dust particles were low (less than 1 %) for both sample types.

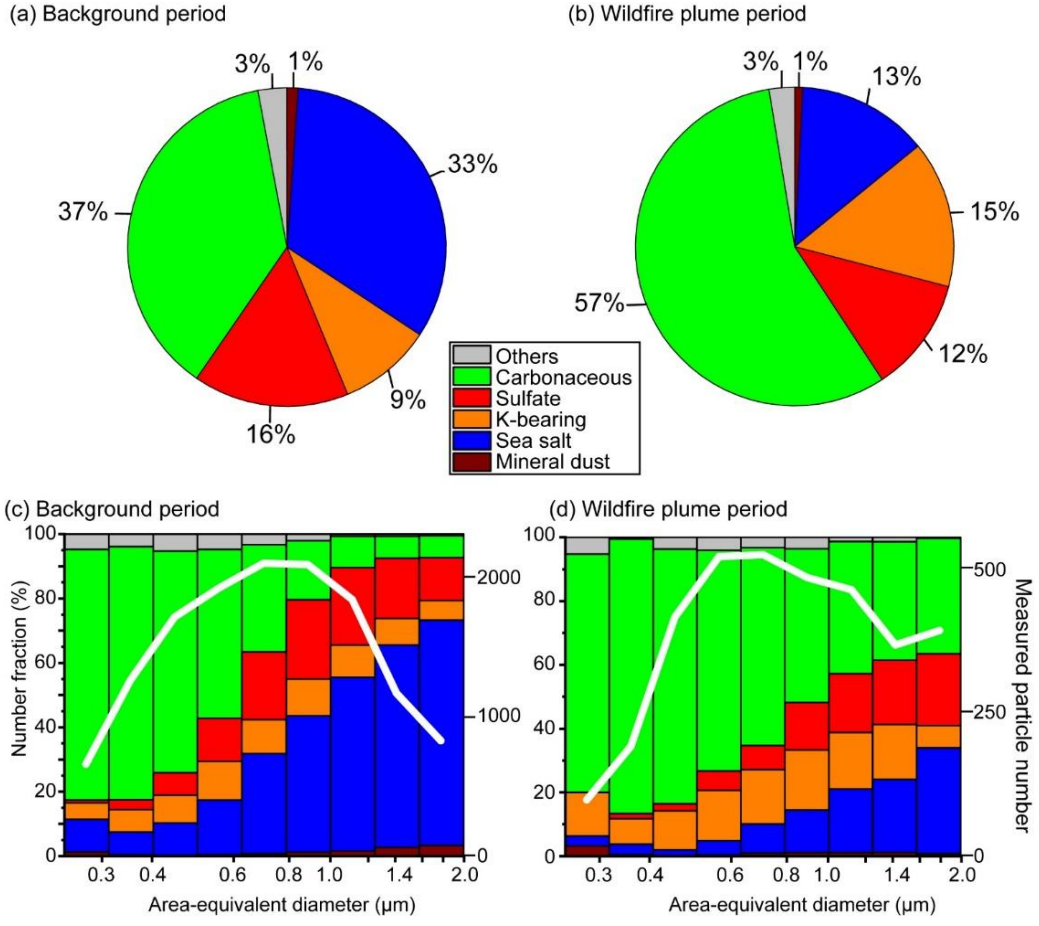

Figure 4. Fractional contribution (a and b) and size-dependence (c and d) of each particle type. (a) and (c): Samples from the background period. (b) and (d): Samples from the wildfire plume period. The lognormal size bin ranges are <0.32, 0.32–0.40, 0.40–0.50, 0.50–0.63, 0.63–0.79, 0.79–1.00, 1.00–1.26, 1.26–1.58, and >1.58 μm in area-equivalent diameter. Note that the area-equivalent diameter tends to be larger than the aerodynamic diameter when particles with low viscosity spread on the substrate. White lines in (c) and (d) indicate particle numbers used for each size bin. N = 13,517 for background samples and 3,400 for wildfire plume samples. The samples from wildfire plume periods were collected from July 5 22:00 to July 8 02:00; from July 17 14:00 to July 18 22:00; and from July 23 14:00 to July 25 02:00 in UTC.

https://doi.org/10.5194/egusphere-2026-3518
Preprint. Discussion started: 3 July 2026

For both background air and wildfire plume samples, the fraction of carbonaceous particles increased with smaller sizes, while the fraction of sea salt particles increased with larger sizes (Figs.4c and 4d). Sulfate fractions generally decreased toward smaller sizes and peaked at ~0.8–1.3 μm for the background samples and at the largest size bin (>1.6 μm) for the wildfire plume samples. K-bearing particle fractions did not differ significantly among size bins. Mineral dust particle fractions increased slightly at sizes larger than 1.3 μm for the background samples. Here, it should be noted that the measured particle fractions were compared along with their area-equivalent diameters among aerosol particles having aerodynamic diameter smaller than 700 nm. The area-equivalent diameter depends on the particle volume and viscosity, whereas the aerodynamic diameter depends on the particle volume, density, and shape, and the volume diameter depends on the particle volume. Thus, particles with low viscosity tend to spread on the substrate and show a larger area-equivalent diameter than their aerodynamic and volume-equivalent diameters. For example, Zhang et al. (2020) showed that the area-equivalent diameter can be nearly two times larger than the volume-equivalent diameter of the same particle. Therefore, although particles larger than 700 nm in area-equivalent diameter were measured, they can still be smaller than 700 nm in aerodynamic diameter.

3.3 Changes in the number and mass fractions of aerosol types over the sampling period

Changes in the number fractions of each aerosol type over the sampling period show that the sea salt, K-bearing, sulfate, and carbonaceous fractions varied significantly depending on the sampling times, whereas the mineral dust fraction remained low. Meanwhile, samples from wildfire plume periods had higher carbonaceous number fractions, ranging from 40 to 80 %, whereas samples from the background period had relatively high sea-salt or sulfate fractions (Fig. 5).

In addition to the number fractions, we estimated the atmospheric mass concentrations of each aerosol type (Fig. 6). $PM_{1.0}$ increased during wildfire plumes 1 and 2 and decreased during and after fog and rain events (e.g., July 16, 18, 20, and 31). During the wildfire plume periods, increases in the mass concentrations of carbonaceous particles (>2.0 μg m^{-3} for all plumes) and K-bearing particles (>1.0 μg m^{-3} for plumes 1 and 2) were observed. These two aerosol species are primarily emitted from wildfires as organic aerosols and potassium salt particles, respectively (Li et al., 2003; Adachi et al., 2025b). The plume from July 17–18 had especially high mass concentrations of both species with maximum values of 9.1 μg m^{-3} for carbonaceous particles and 1.8 μg m^{-3} for K-bearing particles. Additionally, sulfate concentrations were high (> 1.5 μg m^{-3}) in the samples from wildfire plumes 1and 2.

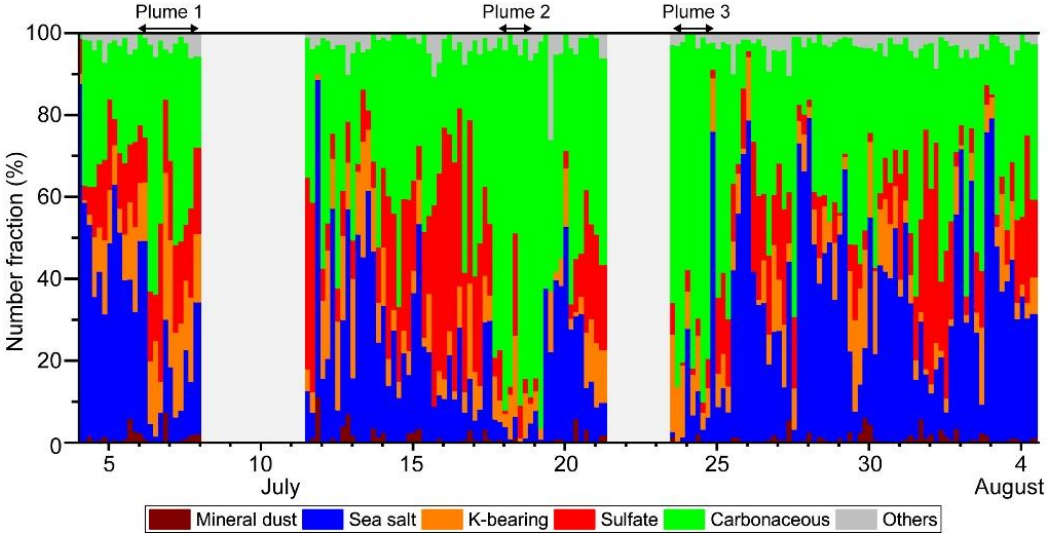

Figure 5. Number fractions of aerosol types within each sample. A total of 155 samples were measured.

https://doi.org/10.5194/egusphere-2026-3518
Preprint. Discussion started: 3 July 2026

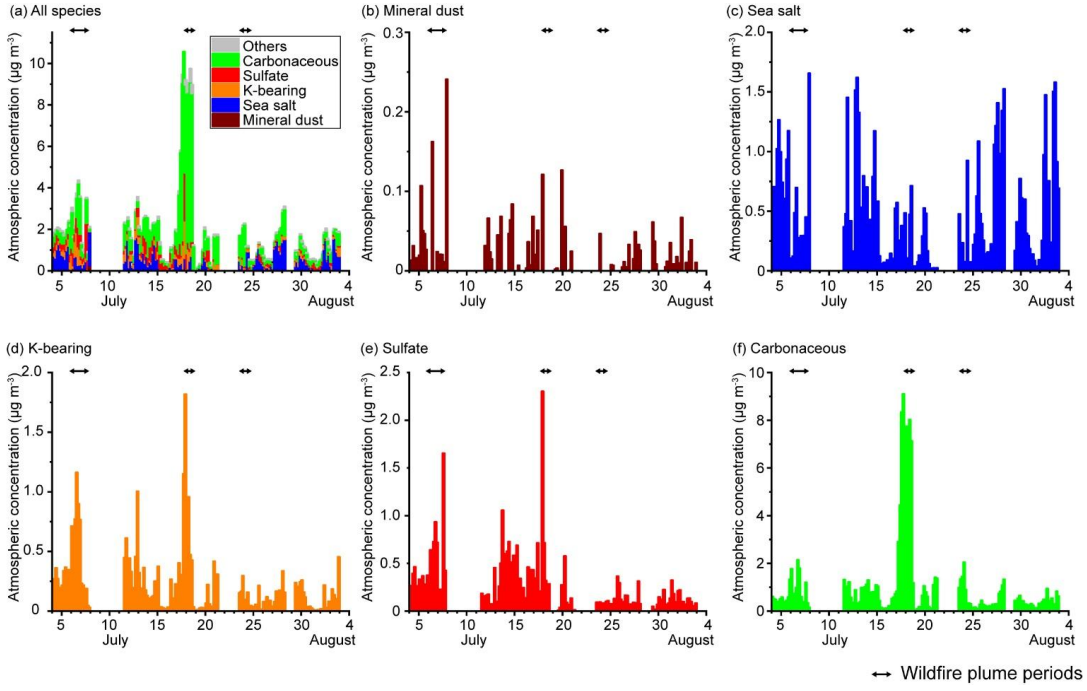

Figure 6. Atmospheric mass concentrations of each aerosol type within $PM_{1.0}$. Data are missing for the following periods: from July 8 2:00 to July 11 14:00; from July 21 10:00 to July 23 14:00; and from July 29 2:00 to July 29 22:00 (UTC).

The concentration of sea salt particles varied greatly from day to day (from 0 to 1.7 μg m^{-3}) due to changes in meteorological conditions. For instance, their concentrations generally increased during periods when the maximum wind speed exceeded 5 m s^{-1}, likely due to wind-driven sea spray emissions (e.g., July 12 and August 2), and generally decreased during fog and rain events due to washout scavenging (e.g., July 16, 18, 20, and 31) (Alden et al., 2026). Sulfate fractions were relatively higher during the first half of the period from July 4 to July 19 than during the second half from July 20 to August 4. Dust particle concentrations were relatively low and showed no apparent peak period in the sampled fine-mode size range.

3.4 Mixing states and composition of individual particles

3.4.1 Particles prevalent in background air

The background air period can be characterized as either sea salt-rich (e.g., July 4–6), sulfate-rich (e.g., July 15–16), or a mixture of the two (Fig. 5). Sea salt and sulfate particles can be either internally mixed, i.e., both S and Na are present in the same particles, or externally mixed, i.e., sea salt and sulfate particles occur as distinct particle types within the same samples (Riemer et al., 2019) (Figs. 7 and 8). Considerable amounts of carbonaceous and K-bearing particles were also present in the background air samples (Fig. 4). These particles possibly originated from stagnant, diluted smoke from the Canadian wildfire (Fig. S1). This hypothesis is supported by the observation of thin organic coatings on sea salt particles (Fig. 7a) and sulfate particles (Fig. 8a), as well as by high fractions of carbonaceous particles in the small particle size ranges of background air samples (Fig. 4c). In addition, a substantial number of vanadium (V)-bearing particles was detected, primarily in background air. A brief discussion of V-bearing particles is provided in the supplementary information (Fig. S2).

During the background periods, the air mass mainly originated from the ocean around Greenland (Fig. 3) and could carry sea salts emitted from the ocean (e.g., on July 4). Sulfate can originate from various sources, including biological activity

https://doi.org/10.5194/egusphere-2026-3518
Preprint. Discussion started: 3 July 2026

in the ocean and long-range transported anthropogenic sources (Schmale et al., 2011, 2022), as well as the stagnant wildfire plumes. The backward trajectory analysis indicates that part of the air mass of the July 16 sample originated from anthropogenic sources in North America (Fig. 3), which could explain the presence of anthropogenic sulfate particles.

Sea salt particles exhibit a mixture of rectangular and needle-like crystal shapes (Fig. 7). These particles primarily contain Na, Mg, Ca, S, O, Cl, and K, suggesting the presence of sodium sulfate and sodium chloride, as well as other salts containing Mg, Ca, and K. Although sulfate and chloride crystals can occur in the same particle, they tend to consist of different grains (Figs. 7a and 7b).

The average composition of each sample indicates that sea salt particles in both the background and the wildfire plume samples had the same Na-to-Mg ratio (Mg/Na = ~0.13) (Fig. 7c). The ratio is almost consistent with the representative Mg/Na value for sea spray aerosols (~0.12) (Seinfeld and Pandis, 2016). In addition, these background samples showed a correlation between Na and Cl (Fig. 7d), suggesting that they were mostly fresh sea salt. Conversely, almost no Cl was detected in sea salt particles from wildfire plume samples. This result suggests that wildfire plumes modify the sea salt composition by replacing Cl with sulfate and other acidic materials, indicating significant chemical processing during the wildfire plume transport.

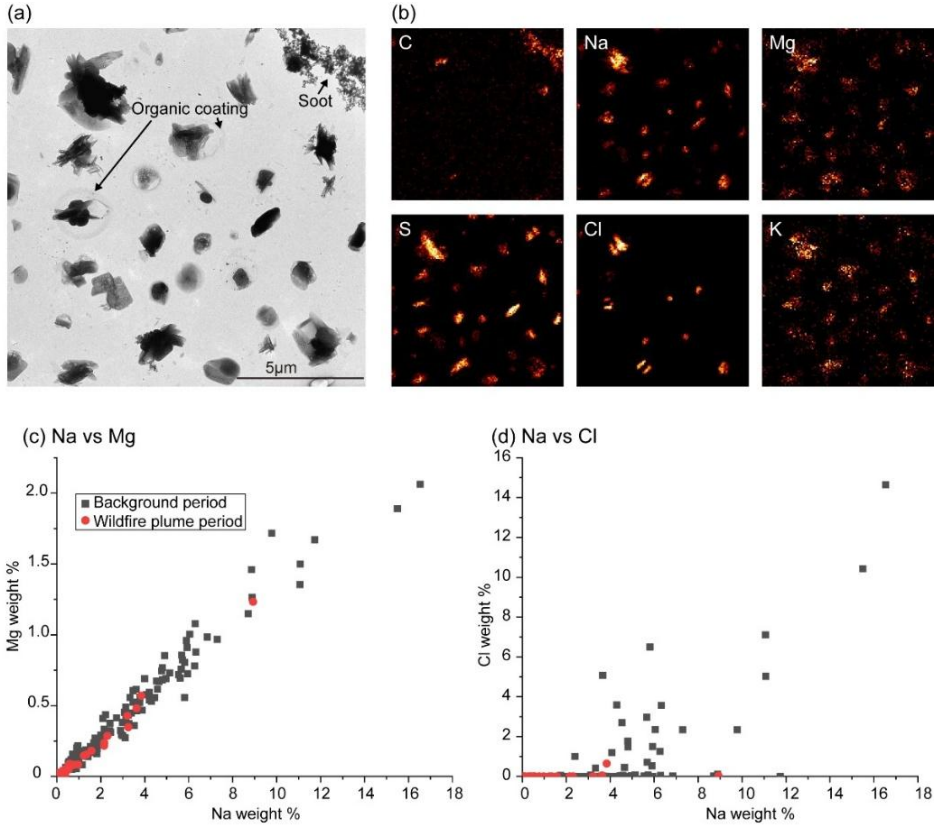

Figure 7. A representative image of sea salt dominant sample and sea salt composition. (a): A transmission electron microscopy image of a sample from the sea salt-dominated background period on July 4 2:00 (UTC). (b): Elemental mapping images of C, Na, Mg, S, Cl, and K in the area shown in the TEM image. (c): Relationship between Na and Mg weight percentages and (d) Na and Cl weight percentages. The sample average values are plotted for the background and wildfire plume periods represented by black squares and red circles, respectively.

https://doi.org/10.5194/egusphere-2026-3518
Preprint. Discussion started: 3 July 2026

In sulfate-rich samples, the sulfate contained both S and N in the same particles and was readily decomposed by exposure to an electron beam (Fig. 8). These results suggest that the particles are ammonium sulfate. Other sulfate-rich samples showed a satellite structure around the sulfate particles (Fig. 8c). These structures are the characteristic appearance of sulfuric acid or ammonium bisulfate, suggesting that they were less neutralized when collected (Okada et al., 2008). Additionally, large soot particles, which possibly originated from local sources such as vehicles, and mineral dust particles are also present in the representative TEM images (Figs. 7a and 8a).

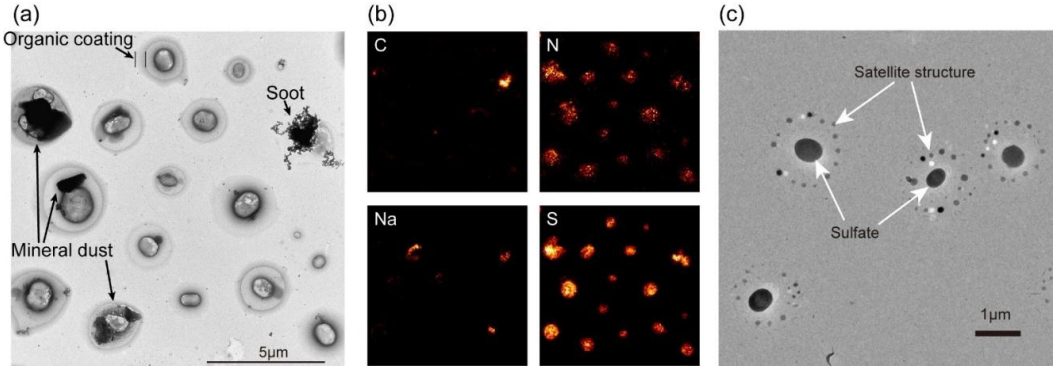

Figure 8. Representative images of sulfate dominant samples and its elemental mapping images. (a): TEM image of a sample collected during the sulfate-dominated background period at 2:00 on July 16 (UTC). (b): Elemental mapping images of C, N, Na, and S for the area shown in (a). (c): Representative transmission electron microscopy image of sulfate particles showing a satellite structure collected at 18:00 on July 14 (UTC).

3.4.2 Particles prevalent in wildfire plumes

Representative images of elemental mapping from the wildfire Plumes 1, 2, and 3 are shown in Fig. 9. These aerosol particles predominantly consist of carbonaceous materials, mainly organic materials, and appear gray due to their amorphous structure and the relatively low atomic numbers of their constituent elements, which are primarily C, N, and O. The presence of N within organic materials suggests that they are a type of organic nitrogen, which are commonly found in aerosol particles from a wildfire plume and may form brown carbon, which absorbs shortwave sunlight (Li et al., 2025; Laskin et al., 2015). They embed other materials, such as soot and potassium sulfate, which decompose upon exposure to a strong electron beam (Fig. 10b). These particles spread over the substrate, indicating low viscosity (liquid phase) at the time of collection.

Potassium sulfate occurs either as a homogeneous mixture with organic materials (Fig. 9a) or as discrete salt grains within organic materials (Figs. 9b and 9c). Similar mixing states of organic-sulfate particles have been observed over the ocean in East Asia, where mixtures of organic material and salt grains were found at high altitudes, whereas homogeneously mixed particles were detected near the ocean surface (Adachi et al., 2025b). A possible explanation for this difference was that the homogeneously mixed particles may have experienced a hydrate phase during transport.

https://doi.org/10.5194/egusphere-2026-3518
Preprint. Discussion started: 3 July 2026

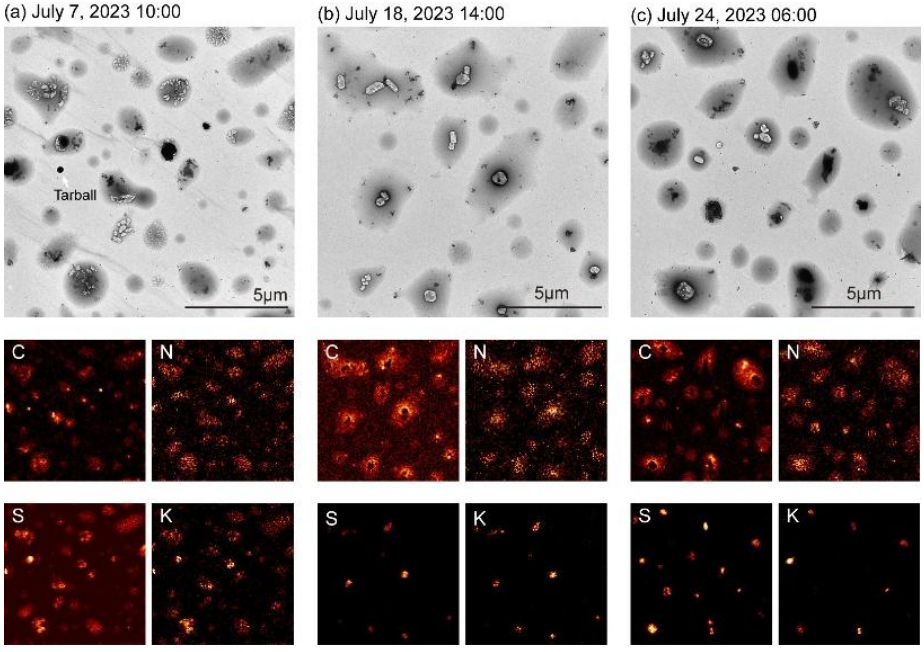

Figure 9. Representative transmission electron microscopy images of samples from wildfire plume periods (top) and their elemental mapping images of C, N, S, and K (bottom). A tarball particle is indicated in image (a). (a): Plume 1. (b): Plume 2. (c): Plume 3.

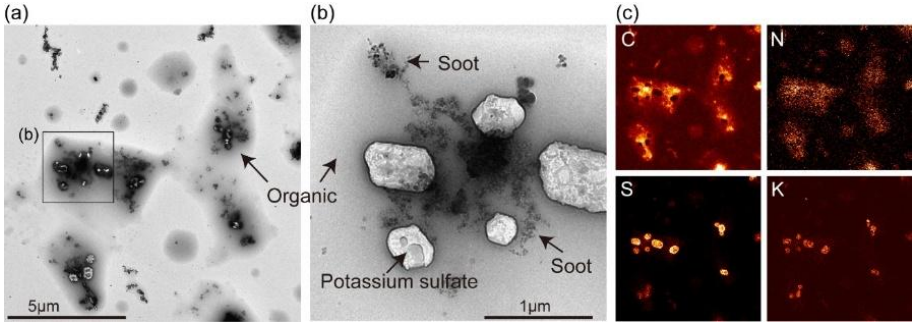

Figure 10. Representative transmission electron microscopy images of a sample from wildfire plume 2 on July 18, 14:00 in UTC (a). (b) A magnified image of the area in (a) after the elemental mapping image analysis. Traces of potassium sulfate particles and embedded soot particles are visible in image (b). (c): Elemental mapping images of C, N, S, and K of the same area.

One or more soot particles, which appear black small dots or aggregates in the TEM images (Figs. 9 and 10), are embedded within the organic material. For example, the sample collected on July 18 contained numerous isolated soot particles dispersed throughout the organic-dominant particles (Fig. 10). These soot particles were ~100–400 nm in length and consisted of several to tens of primary monomer particles. These particles are much smaller than particles without an organic coating, which are several micrometers in size and possibly originate from local sources (Figs. 7a and 8a). Chen et al. (2025) have shown a similar mixture of small soot particles in a wildfire smoke in China. It remains unclear how these small soot particles became mixed with organic material, but it is hypothesized that either small soot particles were embedded in organic materials in the atmosphere, or that larger soot particles broke apart within the host organic materials. Such soot mixing states influence their light absorption properties (Tuccella et al., 2025). The mixing of small soot particles within coating materials can be

https://doi.org/10.5194/egusphere-2026-3518
Preprint. Discussion started: 3 July 2026

better approximated by the Dynamic Effective Medium Approximation (DEMA) with Mie theory than by a core-shell model (Chen et al., 2025). Here, the DEMA model assumes that multiple, small, light-absorbing materials are distributed throughout the host particle, whereas the core-shell model assumes that a single light-absorbing core is located centrally within the host particle. Due to their smaller shadowing effects, scattered soot particles can efficiently absorb sunlight, although this depends on the sizes of the soot and coating materials and the positions of the soot. These small soot particles commonly have a volume-equivalent diameter of less than 60 nm, as estimated from the number (<10) and size (~20 nm in diameter) of their constituent monomers. This size is smaller than the detection limit of instruments that measure black carbon or soot online, such as a single-particle soot photometer (SP2) and particle analysis by laser mass spectrometry (PALMS). The SP2 has a detection limit of ~70 nm, and the PALMS has a detection limit of ~80 nm in volume-equivalent diameter (Moteki and Kondo, 2010; Schwarz et al., 2010; Jacquot et al., 2024). Thus, these instruments may detect such small particles less efficiently or even overlook them, resulting in an underestimation of measured atmospheric black carbon concentrations from wildfires.

Only a small number of tarballs were detected in the current samples (Fig. 9a). Tarballs have been commonly detected in samples from fresh wildfire smoke (less than 24 hours old) from the western US (Chakrabarty et al., 2023; Adachi et al., 2019, 2024). The apparent differences between tarballs and the current organic particles are that the latter are less viscous, deform on the substrate, and are internally mixed with soot particles and various salt crystals. Several hypotheses may explain the reasons why tarballs were hardly detected in the present samples: (1) tarballs were produced in negligible amounts by the Canadian wildfires; (2) tarballs were removed from the atmosphere during long-range transport; and (3) tarballs were transported primarily at higher altitudes—specifically, the main plumes were located at 1–5 km for plume 1 and 1–2 km for plume 2 (Alden et al., 2026)—such that only non-tarball organic particles in the periphery of the plumes reached the surface. These hypotheses cannot be further evaluated in the present study due to the lack of additional samples in the source region and at higher altitudes or relevant observational data.

4. Summary and conclusion

In this study, we collected ambient aerosol particles in southern Greenland during the summer of 2023 as part of the GreenFjord campaign and analyzed them using TEM (STEM-EDS system) to investigate the mixing states and composition of individual particles in the fine mode. During our intensive measurements, we identified and characterized three periods influenced by long-range transport of Canadian wildfire smoke, based on a combination of aerosol mass concentrations, CO concentrations, model analyses, and particle composition. During the wildfire plume periods, K-bearing particles and carbonaceous particles dominated the observed aerosol population, whereas samples collected during the background periods were characterized by higher fractions of sea salt and sulfate particles. In contrast to the abundance of tarballs observed in previous wildfire samples in the western US, the current samples rarely contained them. Instead, the current wildfire plume samples revealed the presence of organic materials internal mixed with potassium sulfate and numerous small soot particles. In addition, wildfire plumes modified sea salt particle composition by replacing chloride with sulfate and other acidic species, indicating chemical processing during transport.

This study showed how large wildfire emissions alter aerosol mixing states and composition in the Arctic. In particular, internally mixed small soot particles embedded within organic matter have important implications for aerosol light absorption. In addition, these internally mixed soot particles can have higher hygroscopicity due to the presence of hygroscopic materials such as sulfate, and exhibit shorter atmospheric lifetime than those without mixing (Oshima et al., 2012). Thus, information about their mixing states improves the estimation of soot deposition on the ice sheet (Thomas et al., 2017). While this study focused on fine-mode aerosol particles, further analysis of coarse-mode aerosol particles with an aerodynamic diameter greater than 700 nm would improve our understanding of naturally occurring, water-insoluble aerosol particles, such as mineral dust particles and bioaerosols, both of which are recognized as important types of ice-nucleating particles.

https://doi.org/10.5194/egusphere-2026-3518
Preprint. Discussion started: 3 July 2026

Overall, this study highlights the significant influence of large wildfires on the population of Arctic aerosol particles and emphasizes the importance of individual particle analysis for accurately characterizing aerosol and climate interactions. As climate change is expected to increase the frequency and intensity of wildfires (Keywood et al., 2013; Abatzoglou and Williams, 2016; Jaffe et al., 2020), the detailed information on aerosol mixing states and aging processes will be useful for improving estimates of aerosol radiative effects, deposition to snow and ice surfaces, and the resulting impacts on the Arctic climate.

Data availability

Data is available at https://doi.org/10.5281/zenodo.20639346 (Adachi, 2026), https://doi.org/10.5281/zenodo.15387460 (Alden et al., 2025), and https://doi.org/10.5281/zenodo.15387340 (Bergner et al., 2025).

Author contributions

KA conducted the TEM analysis and data processing. KA, NB, SO, and YT set up and executed the TEM sampling. NB, JA, and JS measured CO and aerosol size and concentrations. YT and JS supervised and organized the campaign. KA prepared the manuscript with contributions from all coauthors.

Competing interests

At least one of the (co-)authors is a member of the editorial board of Atmospheric Chemistry and Physics.

Acknowledgement

We thank the Narsaq International Research Station team, especially Lise Autogena, and the residents of Narsaq and Narsarsuaq for their generosity, curiosity, and close collaboration throughout our work. We acknowledge the science team members and supporting staff for the GreenFjord campaign. The authors gratefully acknowledge the NOAA Air Resources Laboratory (ARL) for the provision of the HYSPLIT transport and dispersion model and READY website (https://www.ready.noaa.gov) used in this publication. We acknowledge the use of data and imagery from NASA's Fire Information for Resource Management System (FIRMS) (https:// earthdata.nasa.gov/firms), part of NASA's Earth Observing System Data and Information System (EOSDIS).

Financial support.

This research has been supported by the Japan Society for the Promotion of Science (JSPS) KAKENHI program (grant numbers JP23KK0067, JP24H00761, and JP23K28221), the Environmental Research and Technology Development Fund (JPMEERF20232001, JPMEERF20262002) of the Environmental Restoration and Conservation Agency of Japan, the Global Environmental Research Coordination System from the Ministry of the Environment of Japan (MLIT2253), and the Arctic Challenge for Sustainability II (ArCS II) (JPMXD1420318865) and ArCS III (JPMXD1720251001). This work was also supported by funding from the Swiss Polar Institute grant no. SPI-FLAG-2021-002 Greenfjord, the ENAC Flagship 2022 ECO-Plains, and the Swiss National Science Foundation grant no. 200021_212101. This project has received funding from the European Union's Horizon 2020 research and innovation program under grant agreement no. 101003826 via the project CRiceS (Climate Relevant interactions and feedbacks: the key role of sea ice and Snow in the polar and global climate system). J.S holds the Ingvar Kamprad chair for Extreme Environments Research sponsored by Ferring Pharmaceuticals.

https://doi.org/10.5194/egusphere-2026-3518
Preprint. Discussion started: 3 July 2026

References

Abatzoglou, J. T. and Williams, A. P.: Impact of anthropogenic climate change on wildfire across western US forests, Proceedings of the National Academy of Sciences of the United States of America, 113, 11770–11775, 10.1073/pnas.1607171113, 2016.

Adachi, K.: The TEM data used in the figures by Adachi et al obtained during the GreenFjord campaign [Data set]. Zenodo. doi.org/10.5281/zenodo.20639346, 2026.

Adachi, K., Chung, S. H., and Buseck, P. R.: Shapes of soot aerosol particles and implications for their effects on climate, Journal of Geophysical Research: Atmospheres, 115, 10.1029/2009jd012868, 2010.

Adachi, K., Dibb, J. E., Scheuer, E., Katich, J. M., Schwarz, J. P., Perring, A. E., Mediavilla, B., Guo, H., Campuzano-Jost, P., Jimenez, J. L., Crawford, J., Soja, A. J., Oshima, N., Kajino, M., Kinase, T., Kleinman, L., Sedlacek, A. J., Yokelson, R. J., and Buseck, P. R.: Fine ash-bearing particles as a major aerosol component in biomass burning smoke, Journal of Geophysical Research: Atmospheres, 127, 10.1029/2021jd035657, 2022.

Adachi, K., Dibb, J. E., Katich, J. M., Schwarz, J. P., Guo, H., Campuzano-Jost, P., Jimenez, J. L., Peischl, J., Holmes, C. D., and Crawford, J.: Occurrence, abundance, and formation of atmospheric tarballs from a wide range of wildfires in the western US, Atmospheric Chemistry and Physics, 24, 10985-11004, 10.5194/acp-24-10985-2024, 2024.

Adachi, K., Oshima, N., Ohata, S., Yoshida, A., Moteki, N., and Koike, M.: Compositions and mixing states of aerosol particles by aircraft observations in the Arctic springtime, 2018, Atmospheric Chemistry and Physics, 21, 3607-3626, 10.5194/acp-21-3607-2021, 2021.

Adachi, K., Sedlacek, A. J., III, Kleinman, L., Springston, S. R., Wang, J., Chand, D., Hubbe, J. M., Shilling, J. E., Onasch, T. B., Kinase, T., Sakata, K., Takahashi, Y., and Buseck, P. R.: Spherical tarball particles form through rapid chemical and physical changes of organic matter in biomass-burning smoke, Proceedings of the National Academy of Sciences of the United States of America, 116, 19336-19341, 10.1073/pnas.1900129116, 2019.

Adachi, K., Sun, C., Onchang, R., and Takegawa, N.: Homogeneous mixing of sea spray and biomass burning tracer elements within single particles observed over Southeast Asia, Journal of Geophysical Research: Atmospheres, 130, 10.1029/2024jd042328, 2025a.

Adachi, K., Tobo, Y., Oshima, N., Yoshida, A., Ohata, S., Krejci, R., Massling, A., Skov, H., and Koike, M.: Composition and mixing state of individual aerosol particles from northeast Greenland and Svalbard in the Arctic during spring 2018, Atmospheric Environment, 314, 10.1016/j.atmosenv.2023.120083, 2023.

Adachi, K., Yoshida, A., Mori, T., Moteki, N., Ohata, S., Kita, K., Kawai, Y., and Koike, M.: Individual particle compositions and aerosol mixing states at different altitudes over the ocean in East Asia, Atmospheric Chemistry and Physics, 25, 12599–12613, 10.5194/acp-25-12599-2025, 2025b.

Alden, J., Bergner, N., Heutte, B., Weng, J., Violaki, K., Favre, L., & Schmale, J.: Carbon monoxide (CO) measurements in summertime in Narsaq, South Greenland during Greenfjord 2023 [Data set]. Zenodo. https://doi.org/10.5281/zenodo.15387460, 2025.

Alden, J., Bergner, N., Heutte, B., Favre, L., Surdu, M., Weng, J., Augugliaro, M., Winiger, P., Dönmez, B., Pohorsky, R., Calmer, R., Chatterjee, C., Violaki, K., Nenes, A., Gregor, L., Henning, S., and Schmale, J.: Vertically-resolved source contributions to climate-relevant aerosol properties in Southern Greenlandic fjord systems, Atmospheric Chemistry and Physics, 26, 7165–7191, 10.5194/acp-26-7165-2026, 2026.

Andreae, M. O.: Emission of trace gases and aerosols from biomass burning – an updated assessment, Atmospheric Chemistry and Physics, 19, 8523-8546, 10.5194/acp-19-8523-2019, 2019.

Bächler, P., Müller, T. K., Warth, T., Yildiz, T., and Dittler, A.: Impact of ambient air filters on PM concentration levels at an urban traffic hotspot (Stuttgart, Am Neckartor), Atmospheric Pollution Research, 12, 10.1016/j.apr.2021.101059, 2021.

https://doi.org/10.5194/egusphere-2026-3518
Preprint. Discussion started: 3 July 2026

Bergner, N., Alden, J., Heutte, B., Weng, J., Violaki, K., Favre, L., & Schmale, J.: Fidas measurements of total aerosol number concentration and number size distributions in summertime in Narsaq, South Greenland during Greenfjord 2023 [Data set]. Zenodo. https://doi.org/10.5281/zenodo.15387340, 2025.

Bergner, N., Marsh, G., Barry, K., Lacher, L., Böhmländer, A., Alden, J., Ahlqvist, C., Altshuler, I., Bröder, L., Farinotti, D., Favre, L., Guillosson, C., Heutte, B., Höhler, K., Pohorsky, R., Weng, J., and Schmale, J.: Ice-nucleating particles in Greenlandic glacial outwash plains, EGUsphere [preprint], 10.5194/egusphere-2026-484, 2026.

Byrne, B., Liu, J., Bowman, K. W., Pascolini-Campbell, M., Chatterjee, A., Pandey, S., Miyazaki, K., van der Werf, G. R., Wunch, D., Wennberg, P. O., Roehl, C. M., and Sinha, S.: Carbon emissions from the 2023 Canadian wildfires, Nature, 633, 835-839, 10.1038/s41586-024-07878-z, 2024.

Chakrabarty, R. K., Shetty, N. J., Thind, A. S., Beeler, P., Sumlin, B. J., Zhang, C., Liu, P., Idrobo, J. C., Adachi, K., Wagner, N. L., Schwarz, J. P., Ahern, A., Sedlacek, A. J., III, Lambe, A., Daube, C., Lyu, M., Liu, C., Herndon, S., Onasch, T. B., and Mishra, R.: Shortwave absorption by wildfire smoke dominated by dark brown carbon, Nature Geoscience, 16, 683-688, 10.1038/s41561-023-01237-9, 2023.

Chen, X., Ching, J., Wu, F., Matsui, H., Jacobson, M. Z., Zhang, F., Wang, Y., Zhang, Z., Liu, D., Zhu, S., Rudich, Y., Shi, Z., Yoo, H., Jeon, K. J., and Li, W.: Locating the missing absorption enhancement due to multi–core black carbon aerosols, Nature Communications, 16, 10187, 10.1038/s41467-025-65079-2, 2025.

Descals, A., Gaveau, D. L. A., Verger, A., Sheil, D., Naito, D., and Peñuelas, J.: Unprecedented fire activity above the Arctic Circle linked to rising temperatures, Science, 378, 532-537, doi:10.1126/science.abn9768, 2022.

Fang, G.C., Peng, Y.P., Kao, C.L., and Zhuang, Y.J.: Measurements of ambient air fine ($PM_{\leq 2.5}$) and coarse ($PM_{>2.5}$) particulates concentrations by using of a dust monitoring system, Environmental Forensics, 24, 1-8, 10.1080/15275922.2021.1940377, 2023.

Flood, V. A., Strong, K., Whaley, C. H., Chen, J., Wunch, D., Drummond, J. R., Colebatch, O., Gillespie, L., and Mostafavi Pak, N.: The Impact of the 2023 Canadian forest fires on air quality in Southern Ontario, Journal of Geophysical Research: Atmospheres, 130, 10.1029/2024jd042254, 2025.

Freitas, P. G., Adachi, K., Conen, F., Heslin-Rees, D., Krejci, R., Tobo, Y., Yttri, K. E., and Zieger, P.: Regionally sourced bioaerosols drive high-temperature ice nucleating particles in the Arctic, Nature Communications, 14, 5997, 10.1038/s41467-023-41696-7, 2023.

Freitas, P. G., Kopec, B., Adachi, K., Krejci, R., Heslin-Rees, D., Yttri, K. E., Hubbard, A., Welker, J. M., and Zieger, P.: Contribution of fluorescent primary biological aerosol particles to low-level Arctic cloud residuals, Atmospheric Chemistry and Physics, 24, 5479-5494, 10.5194/acp-24-5479-2024, 2024.

Hu, Q., Goloub, P., Veselovskii, I., Podvin, T., Dubois, G., Khaykin, S., Boissière, W., Ducos, F., and Korenskiy, M.: Advanced insights into biomass burning aerosols during the 2023 Canadian wildfires from dual-site Raman and fluorescence lidar observations, EGUsphere [preprint], 10.5194/egusphere-2025-5041, 2025.

Jacquot, J. L., Shen, X., Abou-Ghanem, M., Froyd, K. D., Lawler, M., Schill, G. P., Slovacek, K., Thomson, D. S., Cziczo, D. J., and Murphy, D. M.: A new airborne single particle mass spectrometer: PALMS-NG, Aerosol Science and Technology, 58, 991-1007, 10.1080/02786826.2024.2331549, 2024.

Jaffe, D. A., O'Neill, S. M., Larkin, N. K., Holder, A. L., Peterson, D. L., Halofsky, J. E., and Rappold, A. G.: Wildfire and prescribed burning impacts on air quality in the United States, Journal of the Air & Waste Management Association, 70, 583–615, 10.1080/10962247.2020.1749731, 2020.

Jain, P., Barber, Q. E., Taylor, S. W., Whitman, E., Castellanos Acuna, D., Boulanger, Y., Chavardes, R. D., Chen, J., Englefield, P., Flannigan, M., Girardin, M. P., Hanes, C. C., Little, J., Morrison, K., Skakun, R. S., Thompson, D. K., Wang, X., and Parisien, M. A.: Drivers and Impacts of the Record-Breaking 2023 Wildfire Season in Canada, Nature Communications, 15, 6764, 10.1038/s41467-024-51154-7, 2024.

https://doi.org/10.5194/egusphere-2026-3518
Preprint. Discussion started: 3 July 2026

Keegan, K. M., Albert, M. R., McConnell, J. R., and Baker, I.: Climate change and forest fires synergistically drive widespread melt events of the Greenland Ice Sheet, Proceedings of the National Academy of Sciences of the United States of America, 111, 7964-7967, 10.1073/pnas.1405397111, 2014.

Keywood, M., Kanakidou, M., Stohl, A., Dentener, F., Grassi, G., Meyer, C. P., Torseth, K., Edwards, D., Thompson, A. M., Lohmann, U., and Burrows, J.: Fire in the air: biomass burning impacts in a changing climate, Critical Reviews in Environmental Science and Technology, 43, 40-83, 10.1080/10643389.2011.604248, 2013.

Khaykin, S., Bekki, S., Godin-Beekmann, S., Fromm, M. D., Goloub, P., Hu, Q., Josse, B., Laeng, A., Meziane, M., Peterson, D. A., Pelletier, S., and Thouret, V.: Stratospheric impact of the anomalous 2023 Canadian wildfires: the two vertical pathways of smoke, Atmospheric Chemistry and Physics, 25, 14551-14571, 10.5194/acp-25-14551-2025, 2025.

Kikuchi, K., Taniguchi, T., and Uyeda, H.: Characteristics of the concentration and composition of aerosols during Foehn in West Greenland, Tellus B, 48, 372-386, 10.1034/j.1600-0889.1996.t01-2-00004.x, 1996.

Laskin, A., Laskin, J., and Nizkorodov, S. A.: Chemistry of atmospheric brown carbon, Chemical Revews, 115, 4335-4382, 10.1021/cr5006167, 2015.

Li, J., Pósfai, M., Hobbs, P. V., and Buseck, P. R.: Individual aerosol particles from biomass burning in southern Africa: 2, Compositions and aging of inorganic particles, Journal of Geophysical Research: Atmospheres, 108, 10.1029/2002JD002310, 2003.

Li, Y., Fu, T.-M., Yu, J. Z., Zhang, A., Yu, X., Ye, J., Zhu, L., Shen, H., Wang, C., Yang, X., Tao, S., Chen, Q., Li, Y., Li, L., Che, H., and Heald, C. L.: Nitrogen dominates global atmospheric organic aerosol absorption, Science, 387, 989-995, doi:10.1126/science.adr4473, 2025.

Luo, B., Xiao, C., Luo, D., Fu, Q., Chen, D., Zhang, Q., Ge, Y., and Diao, Y.: Atmospheric and oceanic drivers behind the 2023 Canadian wildfires, Communications Earth & Environment, 6, 10.1038/s43247-025-02387-x, 2025.

Masoom, A., Kazadzis, S., Modini, R. L., Gysel-Beer, M., Gröbner, J., Coen, M. C., Navas-Guzman, F., Kouremeti, N., Brem, B. T., Nowak, N. K., Martucci, G., Hervo, M., and Erb, S.: Long range transport of Canadian Wildfire smoke to Europe in Fall 2023: aerosol properties and spectral features of smoke particles, EGUsphere [preprint], 10.5194/egusphere-2025-2755, 2025.

Matz, C. J., Egyed, M., Xi, G., Racine, J., Pavlovic, R., Rittmaster, R., Henderson, S. B., and Stieb, D. M.: Health impact analysis of PM(2.5) from wildfire smoke in Canada (2013-2015, 2017-2018), Science of the Total Environment, 725, 138506, 10.1016/j.scitotenv.2020.138506, 2020.

McCarty, J. L., Aalto, J., Paunu, V.-V., Arnold, S. R., Eckhardt, S., Klimont, Z., Fain, J. J., Evangeliou, N., Venäläinen, A., Tchebakova, N. M., Parfenova, E. I., Kupiainen, K., Soja, A. J., Huang, L., and Wilson, S.: Reviews and syntheses: Arctic fire regimes and emissions in the 21st century, Biogeosciences, 18, 5053-5083, 10.5194/bg-18-5053-2021, 2021.

Meier, W. N. and Stroeve, J.: An updated assessment of the changing Arctic sea ice cover, Oceanography, 35, 10-19, 2022.

Mouginot, J., Rignot, E., Bjork, A. A., van den Broeke, M., Millan, R., Morlighem, M., Noel, B., Scheuchl, B., and Wood, M.: Forty-six years of Greenland Ice Sheet mass balance from 1972 to 2018, Proceedings of the National Academy of Sciences of the United States of America, 116, 9239-9244, 10.1073/pnas.1904242116, 2019.

Moteki, N., and Kondo, Y.: Dependence of laser induced incandescence on physical properties of black carbon aerosols: measurements and theoretical interpretation, Aerosol Science and Technology, 44, 663-675, 10.1080/02786826.2010.484450, 2010

NASA FIRMS: NRT VIIRS 375 m Active Fire product VNP14IMGT, NASA Atmospheric Science Data Center (ASDC) DAAC [data set], 10.5067/FIRMS/VIIRS/VNP14IMGT_NRT.002, 2025.

Okada, K., Ikegami, M., Zaizen, Y., Tsutsumi, Y., Makino, Y., Jensen, J. B., and Gras, J. L.: Submicrometer sulfur-rich particles in the middle troposphere: Aircraft observations from Australia to Japan, Atmospheric Research, 88, 185-198, 10.1016/j.atmosres.2007.10.012, 2008.

https://doi.org/10.5194/egusphere-2026-3518
Preprint. Discussion started: 3 July 2026

Oshima, N., Kondo, Y., Moteki, N., Takegawa, N., Koike, M., Kita, K., Matsui, H., Kajino, M., Nakamura, H., Jung, J. S., and Kim, Y. J.: Wet removal of black carbon in Asian outflow: Aerosol Radiative Forcing in East Asia (A-FORCE) aircraft campaign, Journal of Geophysical Research: Atmospheres, 117, 10.1029/2011jd016552, 2012.

Rantanen, M., Karpechko, A. Y., Lipponen, A., Nordling, K., Hyvärinen, O., Ruosteenoja, K., Vihma, T., and Laaksonen, A.: The Arctic has warmed nearly four times faster than the globe since 1979, Communications Earth & Environment, 3, 10.1038/s43247-022-00498-3, 2022.

Riemer, N., Ault, A. P., West, M., Craig, R. L., and Curtis, J. H.: Aerosol mixing state: Measurements, modeling, and impacts. Reviews of Geophysics, 57, 187–249. 10.1029/2018RG000615, 2029

Roșu, I.-A., Mourgela, R.-N., Kasoar, M., Boleti, E., Parrington, M., and Voulgarakis, A.: Large-scale impacts of the 2023 Canadian wildfires on the Northern Hemisphere atmosphere, npj Clean Air, 1, 10.1038/s44407-025-00022-9, 2025.

Sato, K., Takahashi, K., and Inoue, J.: Impact of Canadian wildfires on aerosol and ice clouds in the early-autumn Arctic, Atmospheric Research, 315, 10.1016/j.atmosres.2024.107893, 2025.

Schmale, J., Heutte, B., and Dyson, J.: Unveiling the implicit: Arctic coastal aerosol processes, Chimia (Aarau), 78, 748-753, 10.2533/chimia.2024.748, 2024.

Schmale, J., Schneider, J., Ancellet, G., Quennehen, B., Stohl, A., Sodemann, H., Burkhart, J. F., Hamburger, T., Arnold, S. R., Schwarzenboeck, A., Borrmann, S., and Law, K. S.: Source identification and airborne chemical characterisation of aerosol pollution from long-range transport over Greenland during POLARCAT summer campaign 2008, Atmospheric Chemistry and Physics, 11, 10097–10123, 10.5194/acp-11-10097-2011, 2011.

Schmale, J., Sharma, S., Decesari, S., Pernov, J., Massling, A., Hansson, H.-C., von Salzen, K., Skov, H., Andrews, E., Quinn, P. K., Upchurch, L. M., Eleftheriadis, K., Traversi, R., Gilardoni, S., Mazzola, M., Laing, J., and Hopke, P.: Pan-Arctic seasonal cycles and long-term trends of aerosol properties from 10 observatories, Atmospheric Chemistry and Physics, 22, 3067-3096, 10.5194/acp-22-3067-2022, 2022.

Schmale, J., Zieger, P., and Ekman, A. M. L.: Aerosols in current and future Arctic climate, Nature Climate Change, 11, 95-105, 10.1038/s41558-020-00969-5, 2021.

Schwarz, J. P., Spackman, J. R., Gao, R. S., Perring, A. E., Cross, E., Onasch, T. B., Ahern, A., Wrobel, W., Davidovits, P., Olfert, J., Dubey, M. K., Mazzoleni, C., and Fahey, D. W.: The detection efficiency of the single particle soot photometer, Aerosol Science and Technology, 44, 612-628, 10.1080/02786826.2010.481298, 2010.

Sedlacek III, A. J., Buseck, P. R., Adachi, K., Onasch, T. B., Springston, S. R., and Kleinman, L.: Formation and evolution of tar balls from northwestern US wildfires, Atmospheric Chemistry and Physics, 18, 11289-11301, 10.5194/acp-18-11289-2018, 2018.

Seinfeld, J. H. and Pandis, S. N.: Atmospheric chemistry and physics: from air pollution to climate change, 3rd, John Wiley & Sons, 1120 p. 2016.

Sharma, S., Barrie, L. A., Magnusson, E., Brattström, G., Leaitch, W. R., Steffen, A., and Landsberger, S.: A factor and trends analysis of multidecadal lower tropospheric observations of Arctic aerosol composition, black carbon, ozone, and mercury at Alert, Canada, Journal of Geophysical Research: Atmospheres, 124, 14133-14161, 10.1029/2019jd030844, 2019.

Skiles, S. M., Flanner, M., Cook, J. M., Dumont, M., and Painter, T. H.: Radiative forcing by light-absorbing particles in snow, Nature Climate Change, 8, 964-971, 10.1038/s41558-018-0296-5, 2018.

Taketani, F., Tobo, Y., Miyakawa, T., Takigawa, M., Zhu, C., and Kanaya, Y.: Impact of Siberian Wildfires on Ice-Nucleating Particle Concentrations over the Northwestern Pacific, Environmental Science & Technology, 59, 2565-2574, 10.1021/acs.est.4c04889, 2025.

Thomas, J. L., Polashenski, C. M., Soja, A. J., Marelle, L., Casey, K. A., Choi, H. D., Raut, J. C., Wiedinmyer, C., Emmons, L. K., Fast, J. D., Pelon, J., Law, K. S., Flanner, M. G., and Dibb, J. E.: Quantifying black carbon deposition over the

https://doi.org/10.5194/egusphere-2026-3518
Preprint. Discussion started: 3 July 2026

Greenland ice sheet from forest fires in Canada, Geophysical Research Letters, 44, 7965-7974, 10.1002/2017gl073701, 2017.

Tobo, Y., Adachi, K., DeMott, P. J., Hill, T. C. J., Hamilton, D. S., Mahowald, N. M., Nagatsuka, N., Ohata, S., Uetake, J., Kondo, Y., and Koike, M.: Glacially sourced dust as a potentially significant source of ice nucleating particles, Nature Geoscience, 12, 253-258, 10.1038/s41561-019-0314-x, 2019.

Tobo, Y., Adachi, K., Kawai, K., Matsui, H., Ohata, S., Oshima, N., Kondo, Y., Hermansen, O., Uchida, M., Inoue, J., and Koike, M.: Surface warming in Svalbard may have led to increases in highly active ice-nucleating particles, Communications Earth & Environment, 5, 10.1038/s43247-024-01677-0, 2024.

Tuccella, P., Di Antonio, L., Di Muzio, A., Colaiuda, V., Lidori, R., Menut, L., Pitari, G., and Raparelli, E.: Modeling the black and brown carbon absorption and their radiative impact: the June 2023 intense Canadian boreal wildfires case study, Journal of Geophysical Research: Atmospheres, 130, 10.1029/2024jd042674, 2025.

Wang, Z., Wang, Z., Zou, Z., Chen, X., Wu, H., Wang, W., Su, H., Li, F., Xu, W., Liu, Z., and Zhu, J.: Severe global environmental issues caused by Canada's record-breaking wildfires in 2023, Advances in Atmospheric Sciences, 41, 565-571, 10.1007/s00376-023-3241-0, 2023.

Wu, D., Zhang, J., Niu, X., Shi, R., Wang, X., Liu, J., Wen, H., Zhou, Y., Pu, W., Zhang, B., Zhang, D., and Wang, X.: Triggers of the record-breaking 2023 Canadian wildfires: extreme heat waves and droughts driven by abnormally high sea surface temperatures, Journal of Geophysical Research: Atmospheres, 130, 10.1029/2025jd044451, 2025.

Yokelson, R. J., Crounse, J. D., DeCarlo, P. F., Karl, T., Urbanski, S., Atlas, E., Campos, T., Shinozuka, Y., Kapustin, V., Clarke, A. D., Weinheimer, A., Knapp, D. J., Montzka, D. D., Holloway, J., Weibring, P., Flocke, F., Zheng, W., Toohey, D., Wennberg, P. O., Wiedinmyer, C., Mauldin, L., Fried, A., Richter, D., Walega, J., Jimenez, J. L., Adachi, K., Buseck, P. R., Hall, S. R., and Shetter, R.: Emissions from biomass burning in the Yucatan, Atmospheric Chemistry and Physics, 9, 5785-5812, 10.5194/acp-9-5785-2009, 2009.

Yu, P., Toon, O. B., Bardeen, C. G., Zhu, Y., Rosenlof, K. H., Portmann, R. W., Thornberry, T. D., Gao, R.-S., Davis, S. M., Wolf, E. T., de Gouw, J., Peterson, D. A., Fromm, M. D., and Robock, A.: Black carbon lofts wildfire smoke high into the stratosphere to form a persistent plume, Science, 365, 587-590, doi:10.1126/science.aax1748, 2019.

Yumimoto, K., Tanaka, T. Y., Oshima, N., and Maki, T.: JRAero: the Japanese Reanalysis for Aerosol v1.0, Geoscientific Model Development, 10, 3225-3253, 10.5194/gmd-10-3225-2017, 2017.

Zhang, J., Liu, L., Xu, L., Lin, Q., Zhao, H., Wang, Z., Guo, S., Hu, M., Liu, D., Shi, Z., Huang, D., and Li, W.: Exploring wintertime regional haze in northeast China: role of coal and biomass burning, Atmospheric Chemistry and Physics, 20, 5355–5372, 10.5194/acp-20-5355-2020, 2020.

Zhang, S., Solomon, S., Boone, C. D., and Taha, G.: Investigating the vertical extent of the 2023 summer Canadian wildfire impacts with satellite observations, Atmospheric Chemistry and Physics, 24, 11727-11736, 10.5194/acp-24-11727-2024, 2024.

Zhang, Q., Wang, Y., Xiao, Q., Geng, G., Davis, S. J., Liu, X., Yang, J., Liu, J., Huang, W., He, C., Luo, B., Martin, R. V., Brauer, M., Randerson, J. T., and He, K.: Long-range $PM_{2.5}$ pollution and health impacts from the 2023 Canadian wildfires, Nature, 645, 672-678, 10.1038/s41586-025-09482-1, 2025.